nature communications

Article

https://doi.org/10.1038/s41467-024-54488-4

Histone lactylation mediated by Fam172a in POMC neurons regulates energy balance

Received: 11 March 2024

Accepted: 8 November 2024

Published online: 22 November 2024

Check for updates

Zhuo Chen[1,4], Baocheng Wan[1,4], Hong Zhang[1,4], Lina Zhang[2], Rong Zhang[1], Lianxi Li[1], Yi Zhang[1] ✉ & Cheng Hu[1,3] ✉

Glycolysis-derived lactate was identified as substrate for histone lactylation, which has been regarded as a significant role in transcriptional regulation in many tissues. However, the role of histone lactylation in the metabolic center, the hypothalamus, is still unknown. Here, we show that hypothalamic pro-opiomelanocortin (POMC) neuron-specific deletion of family with sequence similarity 172, member A (Fam172a) can increase histone lactylation and protect mice against diet-induced obesity (DIO) and related metabolic disorders. Conversely, overexpression of Fam172a in POMC neurons led to an obesity-like phenotype. Using RNA-seq and CUT&Tag chromatin profiling analyzes, we find that knockdown of Fam172a activates the glycolytic process and increases peptidylglycine α-amidating monooxygenase (PAM), which affects the synthesis of α-MSH, via H4K12la (histone lactylation). In addition, pharmacological inhibition of lactate production clearly abrogates the anti-obesity effect of *PFKO* (*POMC-Cre, Fam172a*$^{loxP/loxP}$, POMC neurons Fam172a knockout). These findings highlight the importance of Fam172a and lactate in the development of obesity and our results mainly concern male mice.

Lactate has traditionally been considered a waste product of glucose metabolism, and is discarded by cells through excretion[1]. However, extensive evidence from recent decades shows that lactate has many diverse roles in physiology, ranging from being a signaling molecule to an energy substrate[2–4]. Lactate plays an important role in energy metabolism. Numerous studies have identified lactate as an important mediator of exercise-induced appetite suppression[5]. As the center of energy regulation, hypothalamic orexigenic/anorexigenic neurons and glial cells express high levels of monocarboxylate transporters (MCTs) that bidirectionally exchange lactate between tissues/cells[6,7], allowing lactate to access intracellular signaling pathways such as the STAT3, Akt and AMPK pathways to control energy balance[8]. Nonetheless, the mechanism of lactate regulation of energy metabolism is still only the tip of the iceberg. Recently, lactate-derived lysine residue lactylation (Kla) was identified as a novel epigenetic modification that plays critical roles in neural excitation and social stress[9], Alzheimer's disease[10], hepatic stellate cell activation and liver fibrosis[11] and myopia[12]. Although these diseases differ, the role of histone lactylation, which is the transcriptional regulation of related genes, is the same. Thus, exploring the potential mechanism of histone lactylation in central hypothalamic metabolism may reveal novel therapeutic strategies for the treatment of obesity.

Family with sequence similarity 172, member A (Fam172a), was first cloned by Li[13]. Subsequently, it was identified that Fam172a is up-regulated by high glucose levels in macrophages and aortic smooth muscle cells[14], suggesting its potential involvement in the pathogenesis of high glucose-induced diseases. However, the functions of cellular Fam172a have not been fully elucidated. In recent years, Bélanger et al. reported that Fam172a plays a key role in variable splicing regulation and cooperative transcription. These researchers proposed a potential mode of action of Fam172a and Chd7 in Ago2-mediated alternative splicing pathway[15]. Nevertheless, the accuracy of this model

[1]Shanghai Diabetes Institute, Shanghai Key Laboratory of Diabetes Mellitus, Shanghai Clinical Center for Diabetes, Shanghai Sixth People's Hospital Affiliated to Shanghai Jiao Tong University School of Medicine, Shanghai, China. [2]School of Public Health, Shanghai Jiao Tong University School of Medicine, Shanghai, China. [3]Department of Endocrinology and Metabolism, Fengxian Central Hospital Affiliated to Southern Medical University, Shanghai, China. [4]These authors contributed equally: Zhuo Chen, Baocheng Wan, Hong Zhang. ✉e-mail: yi.zhang@sjtu.edu.cn; alfredhc@sjtu.edu.cn

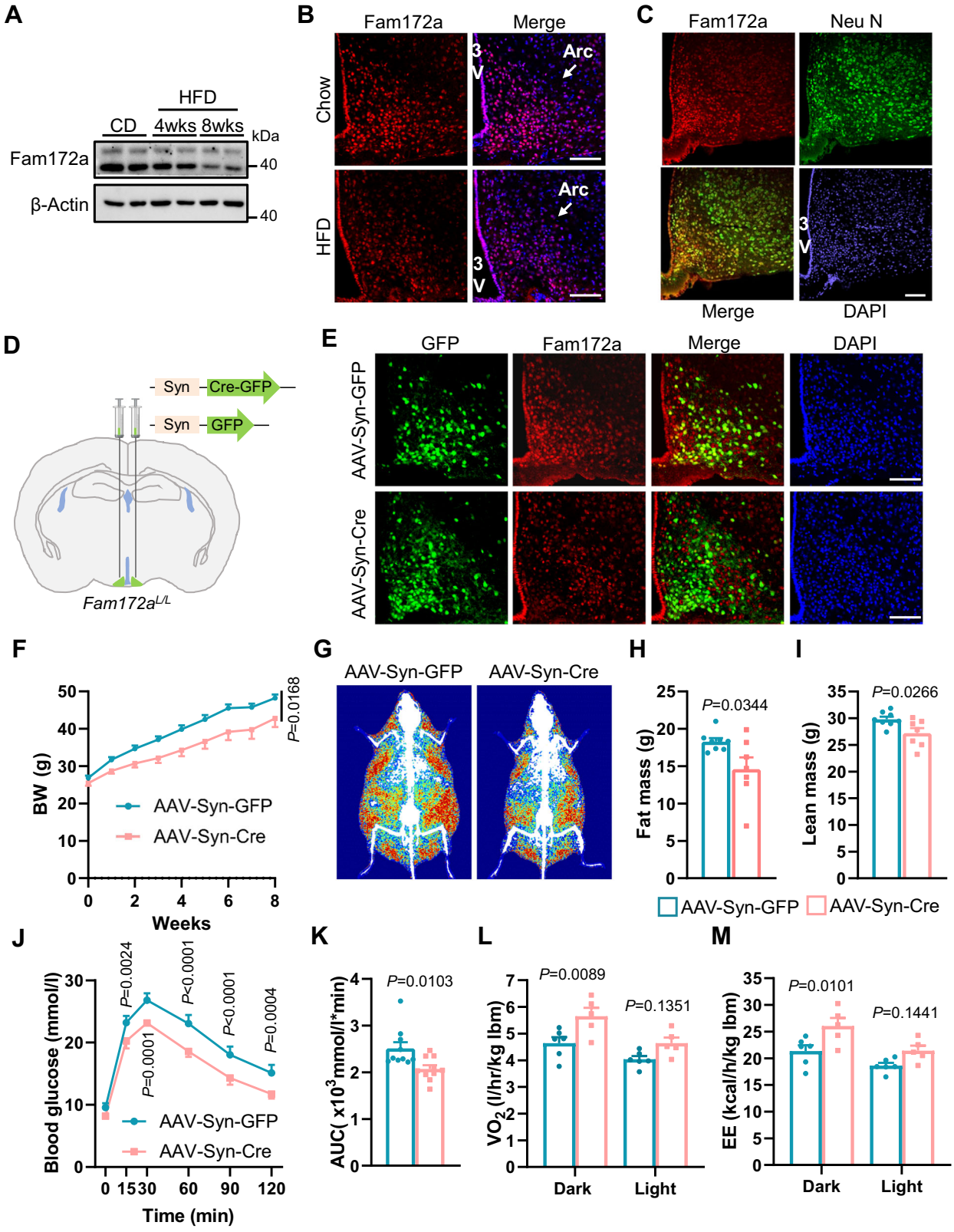

requires further verification through additional evidence. In terms of metabolism, there are few functional studies on Fam172a, therefore, determining where and how this molecule functions remains a major challenge. In this study, we found that Fam172a is more expressed in the hypothalamus among various metabolic tissues. Hence, exploring whether this molecule plays a role in metabolic regulatory center and elucidating its mechanism require further investigation.

The hypothalamus, located in the central nervous system, plays a crucial role in energy balance control[16]. Several neuronal subsets, including pro-opiomelanocortin (POMC) neurons, are important for energy homeostasis[16]. The synthesis and release of α-MSH are integral parts of the function of POMC neurons[17]. In the process of converting POMC to ACTH and then to α-MSH, an amidated peptide, peptidylglycine α-amidating monooxygenase (PAM), the only enzyme that

Fig. 1 | Knockout of Fam172a in the neurons of the hypothalamic Arc protects mice against HFD induced metabolic dysregulation. A Adult *C57 BL/6* mice were fed a chow diet or HFD (4 or 8 weeks), and western blot analysis of Fam172a in Arc of hypothalamus was performed. $n = 3$ mice per group. **B** Expression of Fam172a in Arc of hypothalamus. Brain section of adult *C57 BL/6* mice under a chow diet or HFD 8 weeks were immunostained for Fam172a (red). $n = 5$ mice per group. Cell nuclei were counterstained with DAPI (blue). **Arc**, arcuate nucleus; **3 V**, third ventricle. Scale bars, 100 μm. **C** Expression of Fam172a in Arc of hypothalamus. Brain section of adult *C57 BL/6* mice was coimmunostained for Fam172a (red) and Neu N (green). $n = 4$ mice. Cell nuclei were counterstained with DAPI (blue). **3 V**, third ventricle. Scale bars, 100 μm. **D** Schematic diagram of virus injection in mice. Created in BioRender. Chen, Z. (2024) https://BioRender.com/j97w406. **E** AAV-Syn-GFP and AAC-Syn-Cre were injected into the Arc nucleus of adult *Fam172a*$^{loxP/loxP}$ mice. Immunofluorescence staining for Fam172a (red) and GFP (green) was then performed on brain sections at 4 weeks post-surgery. $n = 4$ mice per group. Cell nuclei were counterstained with DAPI (blue). **3 V**, third ventricle. Scale bars, 100 μm. **F** AAV viruses were injected into the Arc of adult male *Fam172a*$^{loxP/loxP}$ mice fed a HFD. Body weight was then assessed. $n = 8$ mice per group. **G**–**I** AAV viruses were injected into the Arc of adult male *Fam172a*$^{loxP/loxP}$ mice fed a HFD. Representative DEXA images (**G**), fat mass (**H**) and lean mass (**I**) were then assessed. $n = 8$ (AAV-Syn-GFP) or 7 (AAV-Syn-Cre) mice per group. **J**, **K** Glucose tolerance test (GTT, **J**) and the area under the curve (AUC) of the GTT (**K**) of mice. $n = 10$ mice per group. **L**, **M** Oxygen consumption (VO_2, **L**) and energy expenditure (EE, **M**) of the mice. **lbm**, lean body mass; **Dark**, dark cycle; **Light**, light cycle. $n = 6$ (AAV-Syn-GFP) or 5 (AAV-Syn-Cre) mice per group. Data are presented as mean ± SEM. two-tailed Student's *t*-test (**H**, **I**, **K**), two-way ANOVA with Bonferroni's *post hoc* test (**F**, **J**, **L**, **M**). Source data are provided as a Source Data file.

catalyzes this modification, is essential[18]. Additionally, PAM activity requires copper, ascorbate and low pH in the secretory pathway lumen[19], which is consistent with the phenomenon of increased lactate production in the cells of interest. Studies have shown that the PAM is closely related to metabolism, PAM heterozygous older mice displayed increased adiposity and glucose levels compared to wild type controls[20]. Two genome-wide association studies presented the linkage of the PAM to the insulinogenic index and susceptibility to type 2 diabetes[21,22].

In this study, we report that lactate induced H4K12la regulated by Fam172a in POMC neurons mediates dietary obesity. We focused on histone lactylation in hypothalamic neurons. Through genetics, pharmacology, cell molecular biology and other methods, we confirmed that the histone lactylation mediated by Fam172a in POMC neurons can regulate glucose and lipid metabolism. Our research highlights the importance of hypothalamic histone lactylation in the central melanocortin system, providing new directions for the treatment of metabolic diseases.

Results

Knockout of Fam172a in the neurons of the hypothalamic arcuate nucleus (Arc) alleviate high-fat diet (HFD) induced metabolic dysregulation in mice

The Arc of the hypothalamus is considered a key platform for integrating hunger and satiety circulatory signals that reflect energy storage and nutrient availability. Therefore, we investigated the expression and function of Fam172a in the Arc. We employed qRT-PCR to evaluate the expression of Fam172a mRNA in the hypothalamus and other metabolic tissues of male adult *C57 BL/6* mice. The data indicated that Fam172a expressed abundantly in the hypothalamus (Figure S1A). Next, we explored whether Fam172a responds to excess energy in the hypothalamus. The data revealed that the expression level of Fam172a was slight decreased under a HFD 4 weeks, but more decreased under a HFD 8 weeks (Fig. 1A and S1C). In addition, immunofluorescence (Fig. 1B and S1D) and RNAscope (Figures S1E and S1F) were used to confirm that the expression of Fam172a in Arc was decreased in HFD 8 weeks mice. Furthermore, we observed more expression of Fam172a in the neurons of Arc (Fig. 1C and S1B), suggesting that Fam172a may regulate energy balance via its action on these cells.

Next, we injected AAV-Syn-GFP or AAV-Syn-Cre virus into *Fam172a*$^{loxP/loxP}$ mouse Arc (Fig. 1D) via a stereotaxic instrument to establish control mice and neuron specific Fam172a knockout mice. Immunofluorescence (Fig. 1E and S1G) and western blot (Figures S1H and S1I) were used to confirm the success of surgery and the knockdown effect of the virus. As shown in the timeline of the progress of the experiment (Figure S1J), after surgery, the mice were fed with a HFD, at the same time, we monitored the body weights of the animals and other metabolic phenotypes. We observed that Fam172a knockout of neurons in the Arc gained less body weight than the control group (Fig. 1F). Body composition analysis revealed that fat mass and lean mass were both decreased in the AAV-Syn-Cre group (Fig. 1G–I). Moreover, glucose tolerance improved in the knockout mice (Fig. 1J, K). Our indirect calorimetric data showed that AAV-Syn-Cre mice consumed more oxygen and generated more heat during the dark phase (Fig. 1L, M). These findings indicate that knockout Fam172a in neurons of the hypothalamic Arc protects mice from HFD induced obesity, but which neurons play a major role remains to be explored.

Deletion of Fam172a in POMC Neurons Protects Against Diet-Induced Obesity (DIO) and Its Related Metabolic Disorders

As we all know, the hypothalamic arcuate nucleus contains two crucial types of neurons involved in metabolic regulation, one is the orexigenic AgRP neurons and the other is the anorexigenic POMC neurons. Next, we investigated whether Fam172a in AgRP or POMC neurons participates in the regulation of energy balance. By crossing *Fam172a*$^{loxP/loxP}$ mice with *AgRP-Cre* or *POMC-Cre* mice, we generated *AgRP-Cre, Fam172a*$^{loxP/loxP}$ (*AFKO*) mice and *POMC-Cre, Fam172a*$^{loxP/loxP}$ (*PFKO*) mice, with littermate *Fam172a*$^{loxP/loxP}$ mice serving as experimental controls. Immunofluorescence analysis confirmed that Fam172a was successfully knocked out in the POMC neurons of *PFKO* mice (Fig. 2A, B). As shown in the timeline of the progress of the experiment (Figure S2J), subsequently, both *Fam172a*$^{loxP/loxP}$ and *PFKO* mice were fed a HFD. Under this dietary model, the increase in body weight was significantly attenuated in *PFKO* mice compared with controls (Fig. 2C), which was mainly due to reduced adiposity (Fig. 2D–H). Additionally, glucose tolerance (Fig. 2I, J) and insulin sensitivity (Fig. 2K, L) were alleviated in the *PFKO* mice. However, there were no discernible differences between the *Fam172a*$^{loxP/loxP}$ mice and the *PFKO* mice in terms of body weight or glucose tolerance under a chow diet (Figures S2A–S2C). Besides, whether under a chow diet or HFD, there were no significant differences between *Fam172a*$^{loxP/loxP}$ mice and *AFKO* mice in terms of body weight or glucose tolerance (Figures S2D–S2I).

In relation to energy balance, the disruption of Fam172a in POMC neurons reduced appetite in the HFD-fed mice (Fig. 2M). Furthermore, this conditional knockout of Fam172a promoted oxygen consumption and heat production (Fig. 2N, O). We also observed these phenotypes in female *Fam172a*$^{loxP/loxP}$ and *PFKO* mice, and the results were similar (Figure S3A–S3L). These data suggest that Fam172a in POMC neurons mediates obesity and its associated metabolic dysregulation induced by a HFD.

Overexpression of Fam172a in POMC Neurons Leads to an Obesity-Like Phenotype in Chow-Fed Mice

To further explore the function of Fam172a in POMC neurons, we generated an adeno-associated virus (AAV) capable of continuously expressing Fam172a when Cre recombinase is present. Both AAV-GFP virus and AAV-Fam172a virus were bilaterally injected into the Arc of

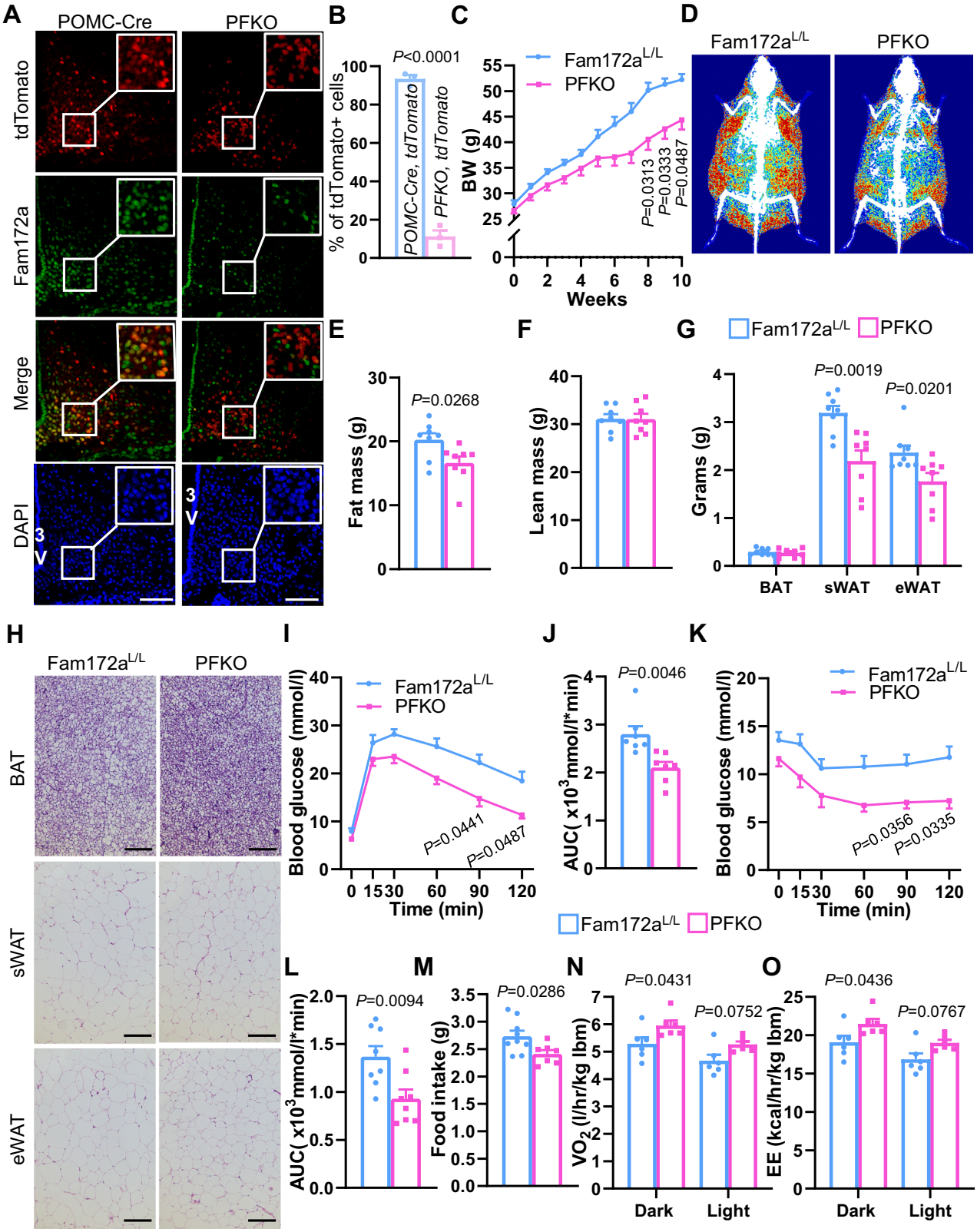

POMC-Cre mice. Immunofluorescence revealed the accurate localization of the virus and overexpression of Fam172a in POMC neurons compared to the control (Fig. 3A). When fed a chow diet, mice administered with AAV-Fam172a gained more body weight and adiposity than the controls, while lean mass did not significantly differ (Fig. 3B–E). Additionally, the mass and size of adipocytes in epididymal white adipose tissue (eWAT) and subcutaneous white adipose tissue (sWAT) were increased (Fig. 3F, G). The constitutive expression of Fam172a in POMC neurons impaired glucose tolerance (Fig. 3H, I) and insulin sensitivity (Fig. 3J, K) in mice. In addition, Fam172a overexpression in mouse POMC neurons increased food intake (Fig. 3L). Moreover, the POMC neurons Fam172a overexpression mice consumed less oxygen and produced less heat than those of the control group (Fig. 3M, N). In summary, these data demonstrate that the

Fig. 2 | Deletion of Fam172a in POMC neurons protects mice against DIO and its associated comorbidities. A, **B** Immunofluorescence staining for Fam172a (green) indicated that Fam172a protein has been depleted from POMC neurons of the *POMC-Cre, Fam172a*$^{loxP/loxP}$ (***PFKO***) mice (**A**) and colocalization quantification of immunofluorescence (**B**). Both *PFKO* and *POMC-Cre* mouse lines were crossed with the *tdTomato reporter/Ai14* mice, so that the POMC neurons could be identified as tdTomato (red)-positive cells in the Arc. Cell nuclei were counterstained with DAPI (blue). **3 V**, third ventricle. $n = 3$ mice per group. Scale bars, 100 μm. **C** Body weight of male mice under HFD feeding. ***Fam172a***$^{L/L}$, *Fam172a*$^{loxP/loxP}$ mice; ***PFKO***, *POMC-Cre, Fam172a*$^{loxP/loxP}$ mice. $n = 8$ (*Fam172a*$^{L/L}$) or 7 (*PFKO*) mice per group. **D**–**F** Representative DEXA images (**D**), fat mass (**E**) and lean mass (**F**) of male mice under HFD feeding. $n = 8$ mice per group. **G** The weights of three adipose tissues, such as BAT, sWAT and eWAT. $n = 8$ mice per group. (**H**) Representative H&E staining images of BAT (upper panel), sWAT (middle panel) and eWAT (lower panel) tissues of the mice fed a HFD. Scale bars, 100 μm. (**I**, **J**) GTT (**I**) and AUC of GTT (**J**) of the mice fed a HFD. $n = 7$ mice per group. **K**, **L** ITT (**K**) and AUC of ITT (**L**) of the mice fed a HFD. $n = 8$ mice per group. (**M**) Average food intake of the mice during HFD feeding. $n = 9$ (*Fam172a*$^{L/L}$) or 7 (*PFKO*) mice per group. (**N**, **O**) Oxygen consumption (VO_2, **N**) and energy expenditure (EE, **O**) of the mice after HFD feeding. **lbm**, lean body mass; **Dark**, dark cycle; **Light**, light cycle. $n = 6$ mice per group. Data are presented as mean ± SEM. two-tailed Student's *t*-test (**B**, **E**, **F**, **G**, **J**, **L**, **M**), two-way ANOVA with Bonferroni's (**C**, **I**, **K**, **N**, **O**). Source data are provided as a Source Data file.

constitutive expression of Fam172a in POMC neurons can lead to an obesity-like phenotype in mice.

Intracellular Lactate Levels are Influenced by Fam172a through Glycolytic Process

To elucidate the function of Fam172a, shRNA constructed as ADV-shFam172a was used to knock down Fam172a. RNA-sequencing was performed in neuro2a cells infected with ADV-shCtrl or ADV-shFam172a. Heatmap analysis showed the top 15 differentially expressed genes, highlighted genes were linked to glycolytic process (Fig. 4A, 4C), which exhibited significant changes in the ADV-shFam172a treated cells. Similarly, Kyoto Encyclopedia of Genes and Genomes (KEGG) pathway analysis revealed notable enrichment of genes related to the glycolytic process pathway following Fam172a knockdown (Fig. 4B).

To further confirm the upregulation of glycolytic process pathway genes in ADV-shFam172a infected cells, qRT-PCR and western blot analyzes were performed. The data demonstrated that the knockdown of Fam172a led to increased mRNA and protein levels of genes crucial for the glycolytic process (Figs. 4D, 4E and S4A). Thereafter, the extracellular acidification rate (ECAR) of the two groups of neuro2a cells were analyzed, and glycolysis (G), glycolytic capacity (GC) and glycolytic rates (GRs) were calculated. The results indicated that the ECAR of the ADV-shFam172a infected group was substantially increased (Fig. 4F, G). Intracellular lactate content was also measured via a Lactate Colorimetric Assay Kit, which revealed that Fam172a knockdown resulted in elevated intracellular lactate levels (Fig. 4H). At present, the structural and functional mechanisms of Fam172a have been mainly studied and reported by Nicolas Pilon's laboratory, which found that Fam172a plays a role in transcriptional regulation in the nucleus[15,23]. In neurons, Fam172a was more highly expressed in the nucleus (Figure S3A). Therefore, we hypothesized that changes in the expression levels of glycolytic process genes were likely related to the transcriptional regulation of these genes. To validate this hypothesis, we determined the promoter activities of lactate dehydrogenase A (LDHA) and pyruvate dehydrogenase kinase 1 (PDK1) through a luciferase assay. The results revealed that the knockdown of Fam172a increased the activity of LDHA and PDK1 promoters (Fig. 4I, J).

Besides, we used CMV-Fam172a plasmid, which can overexpress of Fam172a, to transfect neuro2a cells. qRT-PCR and western blot analyzes were also performed. In contrast, the main mRNAs and proteins levels of the glycolytic process pathway were decreased in the Fam172a overexpressing groups (Figs. 4K, 4L and S4B). Moreover, ECAR and intracellular lactate levels were also decreased (Fig. 4M–O). We subsequently designed a CMV-Fam172a-mNLS[24] plasmid, which overexpresses Fam172a only in the cytoplasm (Figures S4C–S4E). *LDHA* and *PDK1* mRNA levels in neuro2a cells transfected with CMV-Ctrl, CMV-Fam172a or CMV-Fam172a-mNLS were determined, and the data showed that Fam172a overexpression in the cytoplasm had no effect on mRNA expression (Figures S4F and S4G). In summary, Fam172a can regulate lactate levels in neurons through the glycolytic process, which is likely related to its function in the nucleus.

POMC Neurons Knockout of Fam172a Increases Central Lactate Levels through Glycolytic Process

The above results demonstrated that Fam172a knockdown can increase lactate levels through the glycolytic pathway in neuronal cells. However, whether Fam172a knockout has the same effect on POMC neurons of mice needs further verification. Therefore, Seahorse XF Assay was used to determine ECAR of the Arc of hypothalamus tissue from the *Fam172a*$^{loxP/loxP}$ and *PFKO* mice (Fig. 5A). The results showed that the ECAR of PFKO mice was substantially increased (Fig. 5B, C). We also found that Fam172a knockout in POMC neurons increased the protein expression levels of LDHA and PDK1 in the hypothalamic Arc of *PFKO* mice (Fig. 5D and Figure S5A). In addition, the immunofluorescence results further demonstrated that the expression of LDHA and PDK1 were increased in the Fam172a knockout of POMC neurons (Figure S5B–S5E). The lactate content of Arc tissue was increased in *PFKO* mice (Fig. 5E). The above data indicated that POMC neurons knockout of Fam172a could accumulate central lactate levels.

Effect of central administration of lactate on the body energy balance

Next, we investigated whether an increase in brain lactate affects dietary obesity development in mice. To address this question, chow-fed male C57 BL/6 mice were implanted with a cannula directed to the lateral ventricle. After surgical recovery, these mice were switched to an HFD, and received daily treatment with vehicle or lactate through the preimplanted cannula which continued for 2 weeks (Figure S6A). Brain treatment with lactate significantly decreased the body weight and fat mass gains, but did not affect lean mass (Figures S6B–S6D). In addition, lactate treatment alleviated glucose tolerance in mice (Figures S6E and S6F). With respect to energy balance, lactate treatment reduced food intake (Figure S6G). Moreover, this treatment promoted oxygen consumption and heat production (Figures S6H and S6I). Immunofluorescence of cFOS, a marker of neuronal excitability, revealed that lactate treatment could activate POMC neurons (Figure S6J). Hence, central lactate treatment protects mice against HFD-induced body weight gain and associated metabolic disorders.

Inhibition of LDHA Activity Abrogates the Anti-obesity Effect of *PFKO*

We also investigated whether the suppression of brain lactate affects dietary obesity development in *Fam172a*$^{loxP/loxP}$ and *PFKO* mice. To investigate this issue, chow-fed male *Fam172a*$^{loxP/loxP}$ and *PFKO* mice were implanted with a cannula directed to the lateral ventricle. After surgical recovery, these mice were switched to an HFD, and treated with vehicle or oxamate every other day through the preimplanted cannula, which continued for 3 weeks (Fig. 5F). Consistent with our findings, when administered with artificial cerebrospinal fluid (aCSF), *PFKO* mice gained less body weight than that of the *Fam172a*$^{loxP/loxP}$ mice (Fig. 5G). However, inhibition of LDHA activity promoted body weight gain in *PFKO* mice (Fig. 5G). Body composition analysis revealed that fat mass, but not lean mass, was significantly elevated in *PFKO*

https://doi.org/10.1038/s41467-024-54488-4

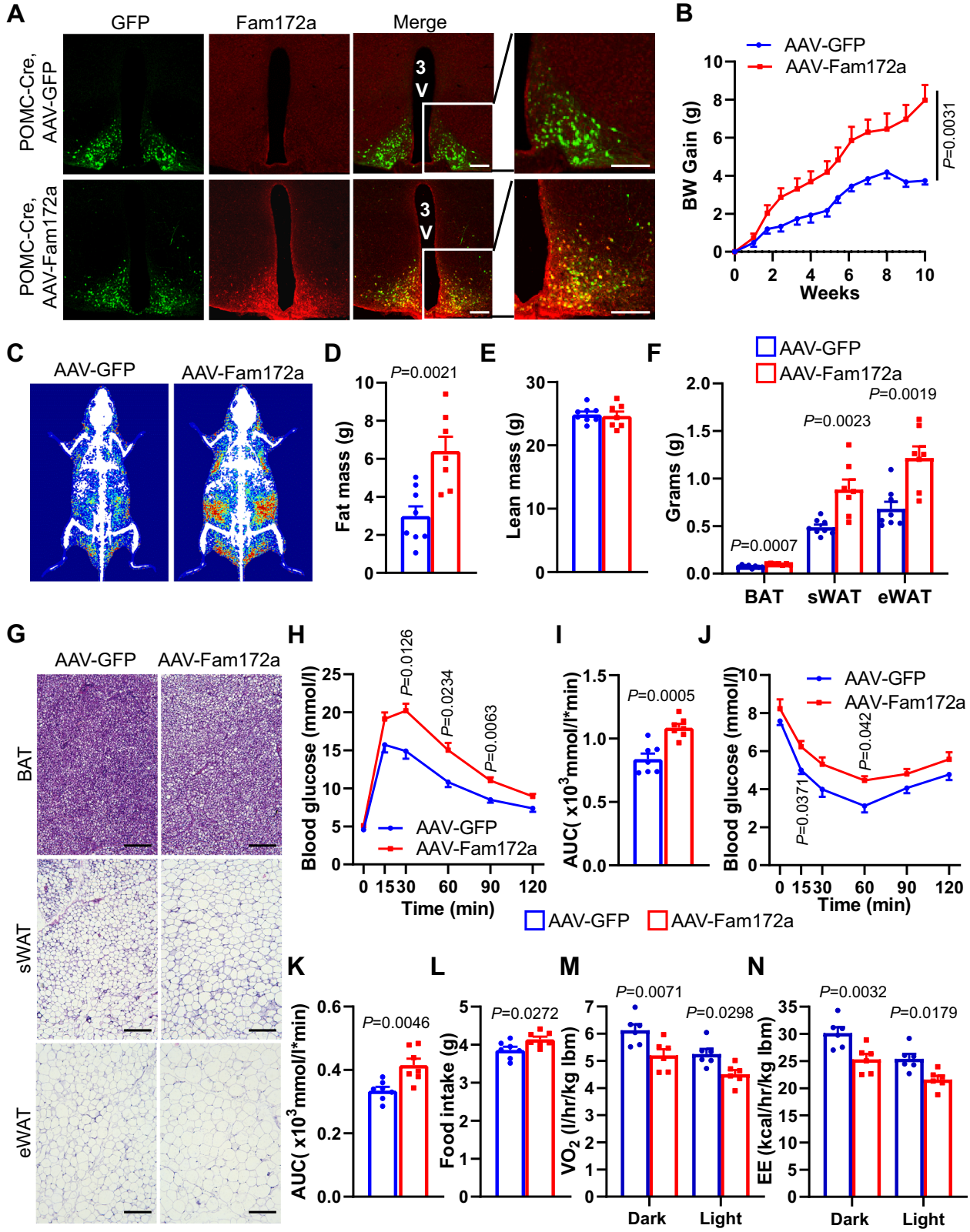

mice treated with oxamate (Fig. 5H–J). Similarly, glucose tolerance was lower in *PFKO* mice treated with oxamate than those treated with aCSF (Fig. 5K, L). In addition, the suppression of LDHA activity increaced the appetite in *PFKO* mice (Fig. 5M). Moreover, this treatment decreased oxygen consumption and heat production of *PFKO* mice (Fig. 5N, O). These data suggest that LDHA mediates the obesity-protective effect in *PFKO* mice.

Inhibition of MCT2 does not affect the function of POMC Neurons with Fam172a Knockout

The lactate transport system is also an important source of increased lactate in POMC neurons, due to the leading monocarboxylate transporter MCT2 expressed[7,25]. Although our previous data did not suggest this pathway, to further demonstrate that the increase in lactate induced by Fam172a knockout in POMC neurons is intracellular, we

Fig. 3 | Activation of Fam172a in POMC neurons leads to an obesity-like phenotype. A AAV-GFP or AAV-Fam172a viruses were injected into the Arc of male adult *POMC-Cre* mice. Immunofluorescence staining for Fam172a (red) was then performed on brain sections. When Cre recombinase is present, infection with the AAV-GFP or AAV-Fam172a virus can lead to GFP expression. $n = 4$ mice per group. Cell nuclei were counterstained with DAPI (blue). 3 V, third ventricle. Scale bars, 100 μm. **B** AAV viruses were injected into the Arc of male adult *POMC-Cre* mice fed a normal chow. Body weight was then assessed. $n = 7$ (AAV-GFP) or 6 (AAV-Fam12a) mice per group. **C**–**E** AAV viruses were injected into the Arc of male adult *POMC-Cre* mice fed a normal chow. Representative DEXA images (**C**), fat mass (**D**) and lean mass (**E**) were then assessed. $n = 8$ (AAV-GFP) or 7 (AAV-Fam12a) mice per group. **F** The weight of three adipose tissues, such as BAT, sWAT and eWAT. $n = 8$ (AAV-GFP) or 7 (AAV-Fam12a) mice per group. **G** Representative H&E staining images of mouse adipose tissues. Scale bars, 100 μm. **H**, **I** GTT (**H**) and the AUC of GTT (**I**) of the mice. $n = 7$ mice per group. (**J, K**) ITT (**J**) and the AUC of ITT (**K**) of the mice. $n = 7$ mice per group. (**L**) Average food intake of the mice was assessed. $n = 7$ mice per group. (**M**, **N**) Oxygen consumption (VO_2, **M**) and energy expenditure (EE, **N**) of the mice. **lbm**, lean body mass; **Dark**, dark cycle; **Light**, light cycle. $n = 6$ mice per group. Data are presented as mean ± SEM. two-tailed Student's *t*-test (**D, E, F, I, K, L**), two-way ANOVA with Bonferroni's *post hoc* test (**B, H, J, M, N**). Source data are provided as a Source Data file.

used inhibitor of MCT2 (AR-C155858) to investigate this pathway[26]. Two groups of mice were subjected to central administration of vehicle or MCT2 inhibitors: chow-fed WT mice and PFKO mice. These mice were implanted with a cannula directed to the lateral ventricle. After surgical recovery, the mice were switched to a HFD, and received treatment of vehicle or AR-C155858 every day through the pre-implanted cannula which continued for 3 days. We found that in WT mice group, the inhibition of MCT2 increased food intake (Figure S7A), and decreased oxygen consumption and heat production (Figures S7B and SC). However, in PFKO mice group, the inhibition of MCT2 had no effect on food intake (Figure S7D), oxygen consumption (Figure S7E) or heat production (Figure S7F). We speculate that in WT mice, the inhibition of MCT2 leads to decreased lactate content within POMC neurons, which inhibits the function of POMC neurons. Although the function of MCT2 was inhibited in the PFKO mice, the knockout of Fam172a in POMC neurons caused an increase in the production of intracellular lactate and therefore did not affect the function of POMC neurons.

Lactate Regulates the Transcriptional Level of PAM through H4K12la

These findings indicate that Fam172a affects POMC neuronal function by regulating lactate levels. Some studies have shown that the increase of lactate accumulation in cells leads to histone lactylation, which might affect the transcriptional regulation of genes. For example, H3K18la or H4K12la are involved in this process[10–12]. Next, we explored which histone lactylation influenced neurons. Immunofluorescence revealed increased expression of H4K12la in neurons of the hypothalamic Arc which could see below. We also detected an increase in H4K12la levels (Fig. 6A and S8A) induced by lactate (25 mM)[9] treatment. To verify the potential functional importance of H4K12la in neurons, we performed genome-wide CUT&Tag analysis to identify candidate genes regulated by H4K12la in neuro2a cells. Briefly, neuro2a cells were treated with NaCl or lactate for 24 h. CUT&Tag using antibodies against H4K12la and analysis with deep Tools[10] showed that the H4K12la peak was more enriched in near transcription start sites (TSSs) in the lactate treated cells than in the control cells (Fig. 6B). The genome-wide distribution of H4K12la indicated that histone modifications were predominantly located within promoter regions (≤ 3 kb), with a 15.74% increase in the lactate-treated group compared with the control group (Fig. 6C). Since the synthesis and release of α-MSH are essential functions of POMC neurons, we focused our attention mainly on the promoters which participate in the synthesis of α-MSH, the called peaks identified PAM, which revealed that the levels of H4K12la at the promoter were significantly elevated (Fig. 6D). Moreover, the mRNA levels and promoter activity of PAM were increased in the Fam172a knockdown cells (Fig. 6E, F). Collectively, these results demonstrate that elevated lactate levels influence PAM gene expression through H4K12la (Fig. 6G).

Besides, RNA sequencing and qRT-PCR of Fam172a knockdown neuro2a cells also showed that the mRNA level of PAM was increased, which was consistent with the results of CUT&Tag analysis (Fig. 6H, I). Subsequently, PAM promoter activity was measured, and Fam172a was knocked down in neuro2a cells. These cells were simultaneously transfected with mouse PAM promoter-driven reporter plasmids. As expected, ADV-shFam172a treatment increased PAM promoter activity (Fig. 6J). In addition, the protein level of PAM was increased in the Fam172a knockdown group (Fig. 6K and S8B). In a previous study, Fam172a knockdown caused an increase in intracellular lactate levels (Fig. 4H). Indeed, western blotting analysis and immunofluorescence of neuro2a cells treated with ADV-shFam172a showed an increase in the level of H4K12la compared with that in the control group (Fig. 6K and S8C–S8E).

Disruption of Fam172a Causes an Increase in Histone Lactylation and α-MSH Release from POMC Neurons

Next, we also examined which type of histone lactylation was influenced by Fam172a knockout in POMC neurons. The immunofluorescence showed H4K12la was increased in the POMC neurons of *PFKO* mice (Fig. 7A–C). Therefore, H4K12la might be more important for the function of Fam172a knockout POMC neurons. The process from POMC to α-MSH requires several crucial enzymes such as PC1/3, PC2, CPE, PAM and PRCP[27]. Thus, we further explored the effects of Fam172a on the α-MSH synthesis pathway. The results of qRT-PCR presented that the mRNA level of *PAM* was increased in the Arc of *PFKO* mice (Fig. 7D). Western blot analysis and immunofluorescence also showed higher expression of PAM in ARC of *PFKO* mice (Fig. 7E and S9A–S9C). We then measured α-MSH levels in the hypothalamus. Immunofluorescence data revealed increased levels of α-MSH in the hypothalamus paraventricular nucleus of hypothalamus (PVN) and dorsomedial hypothalamic nucleus (DMH) of *PFKO* mice (Fig. 7F, G). The data on α-MSH content in the hypothalamus of $Fam172a^{loxP/loxP}$ and *PFKO* mice suggested that POMC neurons Fam172a knockout could increase α-MSH levels in hypothalamus (Fig. 7H) which could suppress appetite. SHU9119, a melanocortin-4 receptor (Mc4r) antagonist, was utilized in a melanocortin system study[28]. Blockade of central melanocortin system via acute intracerebroventricular (i.c.v.) infusion of SHU9119 increased food intake in HFD-fed *PFKO* mice compared with that in the i.c.v. aCSF infused *PFKO* mice. Additionally, SHU9119 treated *PFKO* mice showed no difference compared to i.c.v. aCSF infused control mice (Fig. 7I). Moreover, this treatment decreased oxygen consumption and heat production in *PFKO* mice (Fig. 7J, K). These data suggest that Fam172a regulates the synthesis of α-MSH by affecting the expression of PAM in *PFKO* mice.

Discussion

Fam172a is a novel protein, and its roles and functions in diseases have not been fully elucidated. Previous studies have shown that Fam172a may be involved in the pathogenesis of macroangiopathy[29], carcinoma and CHARGE syndrome[15]. The mechanisms by which Fam172a affects diseases are varied, but a clear conclusion has not yet been reached. In this study, we demonstrated that POMC neuron-specific deletion of Fam172a could alleviate DIO and related metabolic disorders. Conversely, constitutive activation of Fam172a in POMC neurons led to an obesity-like phenotype. Mechanistically, we found that knockdown of

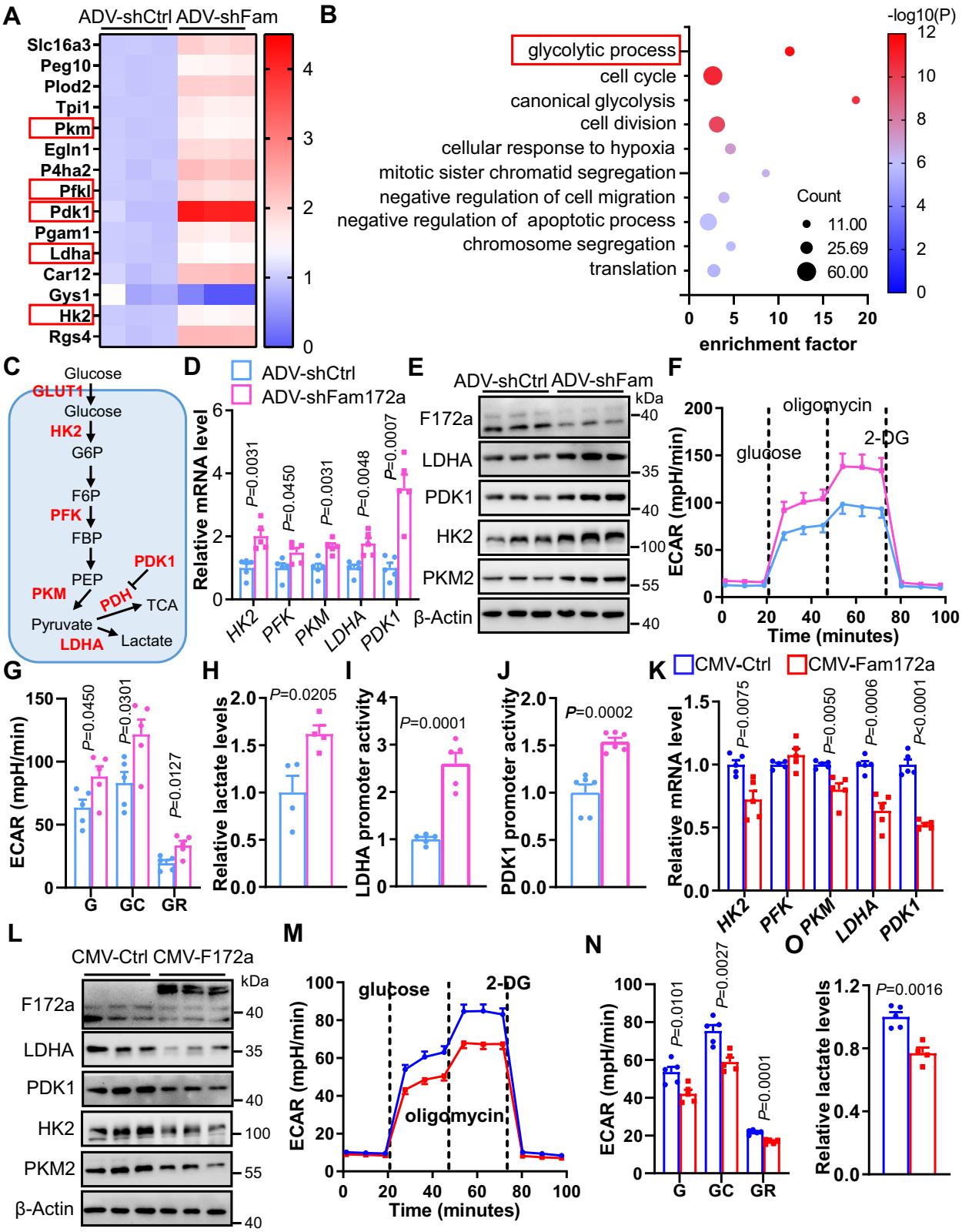

Fam172a increased lactate levels in neuro2a cells, which then promoted H4K12la expression, increasing PAM expression. This pathway was also verified in *PFKO* mice, and the results were consistent. In addition, increased PAM expression led to accelerated synthesis of α-MSH in PFKO mice. Moreover, pharmacological blockade of LDHA to reduce lactate levels obviously abrogated the anti-obesity effect of *PFKO*.

Lactate, once considered a well-known metabolic waste product, is produced by the process of glycolysis. In this process, several enzymes such as HK2, PFK, PKM, PDH, PDK1 and LDHA play key roles from glucose to lactate and pyruvate. Under normal oxygen tension, glucose is processed to pyruvate, which is activated by the enzyme pyruvate dehydrogenase (PDH), or by the inhibition of the pyruvate dehydrogenase kinase isoform (PDK) which phosphorylates PDH and

Fig. 4 | Intracellular lactate levels were increased by glycolytic process after Fam172a knockdown. A, **B** Neuro2a cells were transfected with ADV-shCtrl or ADV-shFam172a at 37°Cfor 48 h, and then RNA-Seq was performed. Heatmaps of the top 15 genes with significant differences (**A**). Top ten KEGG pathways were also shown (**B**). $n = 3$ cell cultures per group. **C** Schematic of the glycolytic pathway, and highlighting (red) the participating enzymes. **D**, **E** Neuro2a cells were transfected with ADV-shCtrl or ADV-shFam172a at 37°C for 48 h, total RNAs or proteins were then extracted, and the relative mRNA (**D**) and protein (**E**) levels of the indicated genes were assessed. $n = 5$ cell cultures per group for qPCR or 3 cell cultures per group for western blot. **F**, **G** Seahorse metabolic analysis (ECAR) of neuro2a cells which were transfected with ADV-shCtrl or ADV-shFam172a at 37°C for 48 h. $n = 5$ cell cultures per group. **H** Intracellular lactate levels of neuro2a cells transfected with ADV-shCtrl or ADV-shFam172a at 37°C for 48 h. $n = 4$ cell cultures per group. **I**, **J** Infection with ADV-shFam172a increased mouse LDHA (**I**) and PDK1 (**J**) promoter activity in Neuro2a cells. $n = 5$ cell cultures per group for LDHA promoter activity analysis or 6 cell cultures per group for PDK1 promoter activity analysis. **K**, **L** Neuro2a cells were transfected with CMV-Ctrl or CMV-Fam172a at 37°C for 48 h, total RNAs or proteins were then extracted, and the relative mRNA (**K**) and protein (**L**) levels of the indicated genes were assessed. n = 5 cell cultures per group for qPCR or 3 cell cultures per group for western blot. **M**, **N** Seahorse metabolic analysis (ECAR) of neuro2a cells transfected with CMV-Ctrl or CMV-Fam172a at 37°C for 48 h. $n = 5$ cell cultures per group. **O** Intracellular lactate levels of neuro2a cells which were transfected with CMV-Ctrl or CMV-Fam172a at 37°C for 48 h. $n = 5$ (CMV-Ctrl) or 4 (CMV-Fam172a) cell cultures per group. Data are presented as mean ± SEM. Hypergeometric test with Bonferroni's *post hoc* test (**B**), two-tailed Student's *t*-test (**D, G, H, I, J, K, N, O**). Source data are provided as a Source Data file.

inhibits its activity, providing carbon atoms for the tricarboxylic acid (TCA) cycle[30]. In contrast, under hypoxic or anoxic conditions, pyruvate is converted to lactate by activation of lactate dehydrogenase (LDH) in a process known as anaerobic glycolysis[31]. However, aerobic glycolysis also exists, which was initially described in cancer cells by Otto Warburg[32], and lactate is formed despite the presence of normal oxygen tension. In addition, active brain tissue also undergoes aerobic glycolysis, which does not completely oxidize glucose but instead produces local excess lactate, one of the main sites being astrocytes[33], in which the expression of genes that promote glycolysis such as PFKFB3, PKM2, PDK4 and LDHA/B upregulated[34], and the expression profiles favor aerobic glycolysis. In this work, we discovered that Fam172a knockdown could increase the expression of genes associated with glycolytic pathways in neurons, especially LDHA and PDK1, thereby regulating lactate levels. Our data also suggest that this increase may be due to the effect of Fam172a on promoter activity, although the specific mechanism needs to be further explored.

Many studies have explored the hypothesis that lactate could play a role in inducing satiety through hypothalamus[28,35]. Researchers subsequently focused on the lactate delivery system, specifically for POMC neurons. Tanyocytes, owing to their unique anatomical location, can acutely sense glucose in the cerebrospinal fluid and then convert brain glucose supplies into lactate, which they transmit through MCTs to arcuate POMC neurons, integrating this signal to drive their activity and adapt to the metabolic response to meet physiological demands[25,36]. Astrocyte was famous for its function to regulate glucose uptake and lactate release, a mechanism known as the astrocyte neuron lactate shuttle[37], which can activate POMC neurons to release α-MSH[38]. Ou et al. reported that oligodendrocytes GPR17 could regulate lactate production through PDK1, and that increased lactate activates AKT and STAT3 signaling in hypothalamic neurons, leading to increased expression of POMC and suppression of AgRP[8]. Yoon et al. reported that lactate affects redox signaling through mitochondrial mechanisms related to uncoupling protein 2 (UCP2) and lipid utilization in the hypothalamic anorexigenic POMC neurons to regulate feeding and peripheral glucose metabolism[39]. The above studies showed that lactate could activate POMC neurons to regulate the body's metabolism, but the source of lactate is the transfer of surrounding glial cells. However, our study found that blocking MCT2 transport lactate to POMC neurons in PFKO mice did not affect the function of POMC neurons, indicating that Fam172a in neurons regulated intracellular lactate levels through glycolytic pathway which was different from previous studies, and subsequently induced histone lactylation.

Histone lactylation was recently identified as an epigenetic modification that is regulated by intracellular lactate content, and similar to histone methylation, histone lactylation can directly stimulate gene transcription from chromatin[40]. During physiological processes, histone Kla sites, including H3K18la or H4K12la, play important roles in M1 macrophage polarization[41], hepatic stellate cell activation[11], neural development[10] and the development of myopia[12]. The mechanisms by which histone Kla regulates cell fate transition in physiological processes are likely associated with promoter binding and gene expression. In this study, we found that H4K12la was more expressed than H3K18la in neurons, and that H4K12la was increased in Fam172a knockout POMC neurons. Therefore, we mainly studied the role of H4K12la in neurons. Similar to the above studies, we focused on whether the transcriptional function of H4K12la involved in POMC to α-MSH pathway. Interestingly, in lactate treated neuro2a cells, through CUT&Tag analysis, we found that the H4K12la peak was enriched in POMC and PAM promotors which could regulate the synthesis of α-MSH, but more enriched in the promotor of PAM in the Fam172a knockdown group than the control group. We also validated the activity of PAM promoter via a dual luciferase reporter assay. In conclusion, we discovered that Fam172a could regulate the synthesis of α-MSH by affecting the expression of PAM through lactate induced H4K12la in PFKO mice.

Limitations

Our study revealed that knockdown of Fam172a activated glycolytic process which resulted in H4K12la, increased PAM expression via H4K12la, and ultimately regulated the energy balance. However, several limitations should be noted. First, research techniques on histone lactation modification are limited at present. For example, we can detect a positive correlation between lactate levels and histone lactylation, but there is no technical method to accurately quantify the key enzyme lactyl-CoA, which is involved in cellular protein lactylation. Another limitation is that we could not isolate POMC neurons from the hypothalamic Arc or perform CUT&Tag analysis, which might more accurately reveal the molecular mechanism of POMC neurons.

Methods

Study approval

Animal procedures were approved by the Institutional Animal Care and Use Committee of Shanghai Sixth People's Hospital Affiliated to Shanghai Jiao Tong University School of Medicine, and the animal welfare ethics acceptance number is No: 2022-0291.

Animals

The *Fam172a*$^{loxP/loxP}$ mice were kindly provided by Dr. Lianxi Li (Shanghai Sixth People's Hospital affiliated to Shanghai Jiao Tong University School of Medicine). *POMC-Cre*[42] and *tdTomato reporter/Ai14* mice[43] were generated as previously described. Male *C57 BL/6* mice were purchased from GemPharmatech Co., Ltd. (Nanjing, China). The animals were housed under a 12 h light/12 h dark cycle in a temperature-controlled room (22-24°C) and had ad libitum access to water and food, except where noted. Rodent chow (11.1% kcal from fat) diet were purchased from Xietong Bioscience (1010097, Beijing, China) and high-fat diet (60% kcal from fat) were purchased from

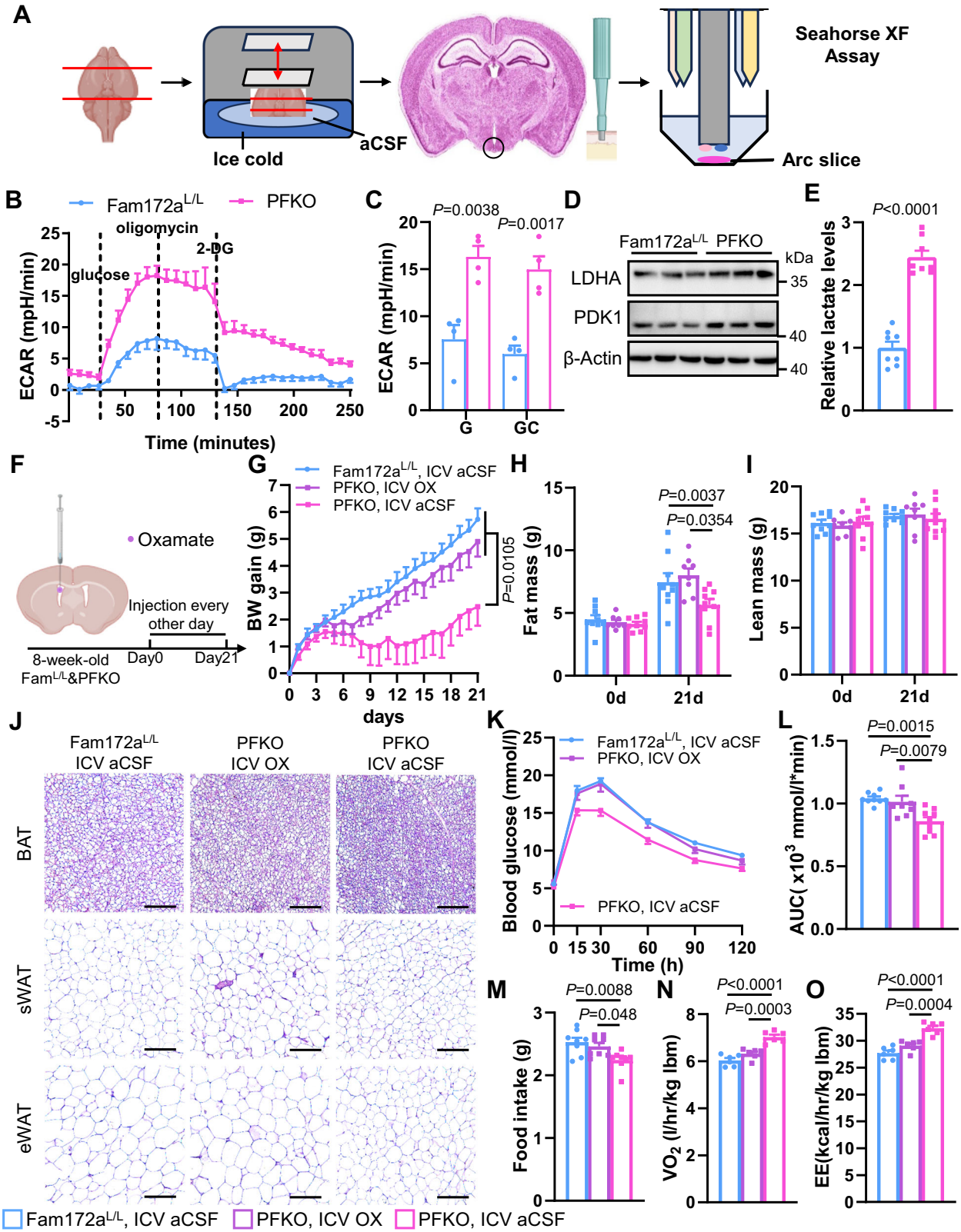

Research Diets (D12492, New Brunswick, NJ, USA), respectively. The DIO model mice were fed a HFD for 14 weeks starting at age of 8 weeks, unless otherwise noted. To ensure animal welfare, we observe mice every day, and if there were changes in physical condition such as abnormal coat condition or posture, lameness, loss of body weight, and excessive licking or scratching of any mice, we will give more frequent observations. Humane endpoint was set includes excessive reduced locomotor activity (inability to access food and water), dehydration, and excess weight loss (>20% of body weight) within a few days. Since our mice models and experiment schedule, we did not observe any mice reached the humane endpoint. At the end of the experiment (for DIO mice: HFD for 2–24 weeks; for CD mice: feeding for 8-32 weeks), mice were euthanized via CO_2-dependent asphyxiation and tissues were harvested.

Fig. 5 | Inhibition of LDHA activity abrogates the anti-obesity effect of PFKO. **A** Schematic diagram of the Seahorse XF Assay test of the hypothalamus Arc. Created in BioRender. Chen, Z. (2024) https://BioRender.com/j97w406. **B**, **C** Seahorse metabolic analysis (ECAR) of hypothalamus Arc in Fam172A$^{L/L}$ or PFKO mice. $n = 4$ mice per group. **D** Western blot analysis of LDHA and PDK1 in hypothalamus Arc of *Fam172A*$^{L/L}$ or *PFKO* mice. $n = 3$ mice per group. **E** Intracellular lactate levels of hypothalamus Arc in *Fam172A*$^{L/L}$ or *PFKO* mice. $n = 8$ mice per group. **F**, **G** Adult male *Fam172a*$^{L/L}$ or *PFKO* mice were fed a chow diet, and were then placed cannula directed to lateral ventricle. After 2 wks of recovery, mice were switched from chow diet to HFD and were i.c.v. administered aCSF or oxamate every other day for 21 days (**F**), created in BioRender. Chen, Z. (2024) https://BioRender.com/j97w406. Body weight gain (**G**) was assessed. $n = 8$ (Fam12a$^{L/L}$, ICV aCSF) or 9 (PFKO, ICV OX) or 10 (PFKO, ICV aCSF) mice per group. **H**, **I** Fat mass (**H**) and lean mass (**I**) of treated mice were also assessed. $n = 8$ (Fam12a$^{L/L}$, ICV aCSF) or 9 (PFKO, ICV OX) or 9 (PFKO, ICV aCSF) mice per group. **J** Representative H&E staining images of mouse adipose tissues. Scale bars, 100 μm. **K**, **L** After oxamate treatment, the mice were subjected to the GTT (**K**). The AUC (**L**) of GTT is shown. $n = 9$ (Fam12a$^{L/L}$, ICV aCSF) or 8 (PFKO, ICV OX) or 9 (PFKO, ICV aCSF) mice per group. **M** Average food intake assessed during the treatment period. $n = 8$ mice per group. **N**, **O** Central administration of oxamate decreased oxygen consumption (VO2, **N**), and energy expenditure (EE, **O**) in PFKO mice. lbm, lean body mass. $n = 6$ mice per group. Data are presented as mean ± SEM. two-tailed Student's *t*-test (**C, E**), one-way ANOVA with Turkey's *post hoc test* (**L, M, N, O**), two-way ANOVA with Bonferroni's *post hoc* test (**G, H, I, K**). Source data are provided as a Source Data file.

Plasmid construction and virus production

The constitutive Fam172a-flag expression plasmid was obtained from Dr. Lianxi Li. The Fam172 gene were first cloned and inserted into AAV-EF1α-DIO-Fam172a-EGFP. The Cre-inducible, EGFP-expressing plasmid AAV-EF1α-DIO-EGFP was used as an experimental control. The plasmids were subsequently sent to a company, and both AAVs were produced by Vigene Biosciences (Jinan, China). ADV-shFam172a and ADV-shCtrl were produced by Obio Technology Corp., Ltd. (Shanghai). For generation of a promoter-reporter plasmid, mouse LDHA promoter (NCBI reference sequence: NC_000073.7, region: 46490198-46491698, complement) and mouse PAM promoter (NCBI reference sequence: NC_000067.7, region: 98025578-98023478, complement) were synthesized by Tsingke Bio, and then were inserted into pGL3-Basic (Promega, Madison, WI) between the NheI and HindIII sites respectively. Successful construction of plasmid was verified by DNA sequencing. The pGL3-Basic-PDK1(mouse)-promoter was purchased from Miaoling Bio.

Stereotaxic surgery

The procedures are based on a previous article published by our team[44]. To inject viruses into Arc nucleus, the mice were anesthetized with avertin (300 mg kg-1), and were then placed on an ultra-precise stereotaxic instrument (RWD, Shenzhen, China). With the help of a micro syringe pump (KD Scientific, Holliston, USA), viral solution was bilaterally injected into Arc at coordinates 1.8 mm posterior to, 0.2 mm lateral to, and 5.8 mm below the surface of the skull. Lateral ventricle cannulation[45]: mice were anesthetized and then placed on the stereotaxic instrument. A 28 G guide cannula was implanted at the coordinates 0.6 mm posterior to bregma, 2.0 mm below the surface of the skull, and 1 mm lateral to the bregma. Mice were allowed to recover for 2 weeks before any further procedures were performed.

Body weight and food intake measurements

Mice were separated into single cages at 8 weeks of age, and their food intake and body weight were monitored. When differences in food intake appeared, the animals were fed in combined cages, but their body weight was still monitored as a single animal. Body weights of mice were measured once a week. Food intake was measured on a daily basis.

Measurement of metabolic parameters

Body composition was measured via DEXA (InAlyzer, Seoul, South Korea) or Minispec LF50 body composition analyzer (Bruker, Rheinstetten, Germany). Oxygen consumption and energy expenditure were assessed via the Laboratory Animal Monitoring System (Columbus, St Paul, USA), and were normalized to lean body mass (lbm).

Glucose tolerance test (GTT)

Mice were fasted overnight, and were then intraperitoneally administered with D-glucose (2 g kg-1). Blood glucose was measured using a glucometer (Roche, Basel, Switzerland) at various time points (0, 15, 30, 60, 90 and 120 min).

Insulin tolerance test (ITT)

Mice were fasted from 8:00 am to 14:00 pm, and then intraperitoneally administered insulin (1.5 g kg-1). Blood glucose was measured via a glucometer (Roche, Basel, Switzerland) at various time points (0, 15, 30, 60, 90 and 120 min).

Immunofluorescence

Mice were anesthetized via Avertin, and fixed with 4% paraformaldehyde (PFA) through transcardial perfusion. Brain tissues were cryoprotected with 20% and 30% sucrose solutions, and then sectioned on a cryostat. Tissue sections were blocked with 5% serum/0.3% Triton X-100/PBS, and incubated with rabbit anti-Fam172a (1:400, Abcam, ab121364), anti-H4K12la (1:200, PTM Bio, PTM-1411RM), anti-H3K18la (1:200, PTM Bio, PTM-1406RM), anti-LDHA (1:200, Proteintech, 1998-1-AP), anti-PDK1 (1:200, Abcam, ab202488), anti-PAM (1:200, Abcam, ab237488) or anti-cFos (1:500, Synaptic Systems, 226308), and sheep anti-α-MSH (1:1000, Millipore, Ab5087), and chicken anti-GFP (1:200, Abcam, ab13970), primary antibodies at 4°C overnight, and with fluorophore-conjugated secondary antibodies (Thermo Fisher, Waltham, MA) at room temperature for 1 hour. Images were acquired with an LSM980 confocal microscope (Carl Zeiss, Jena, Germany) or a FluoView FV1200 confocal microscope (Olympus, Tokyo, Japan), and were processed via ImageJ (NIH, Bethesda, MD).

Hematoxylin and eosin (H&E) staining

sWAT, eWAT and brown adipose tissue (BAT) tissues were harvested, fixed in 4% polyformaldehyde, and then embedded in paraffin. Tissues were sectioned at a thickness of 5 μm and sequentially stained with H&E solutions. Images were collected on an AE31 brightfield microscope (Motic, Xiamen, China).

Cell culture

Neuro2a cells (ATCC, CCL-131) were transfected with CMV-Ctrl and CMV-Fam172a plasmids, or ADV-shCtrl and ADV-shFam172a virus at 37°C for 48 h, and then harvested. Total protein and RNA were extracted for western blot and qRT-PCR analyzes. In a separate experiment, neuro2a cells were treated with NaCl or lactate (25 mM) for 24 h[9]. Total proteins and RNAs were extracted for further analyzes.

Quantitative RT-PCR

Total RNA was extracted from Neuro2a cells via TRIzol reagent (Thermo Fisher). Complementary DNA was synthesized via an RT reagent kit (Takara). RT-PCR was performed using SYBR Green Premix (Thermo Fisher) on a QuantStudio 7 Flex Real-Time PCR System (Thermo Fisher). We used the $2^{-\Delta Ct}$ method to determine the relative RNA level, where ΔCt is the difference between the Ct value of a given gene and that of the *β-Actin* control. Sequences of primers were provided in Supplementary Data.

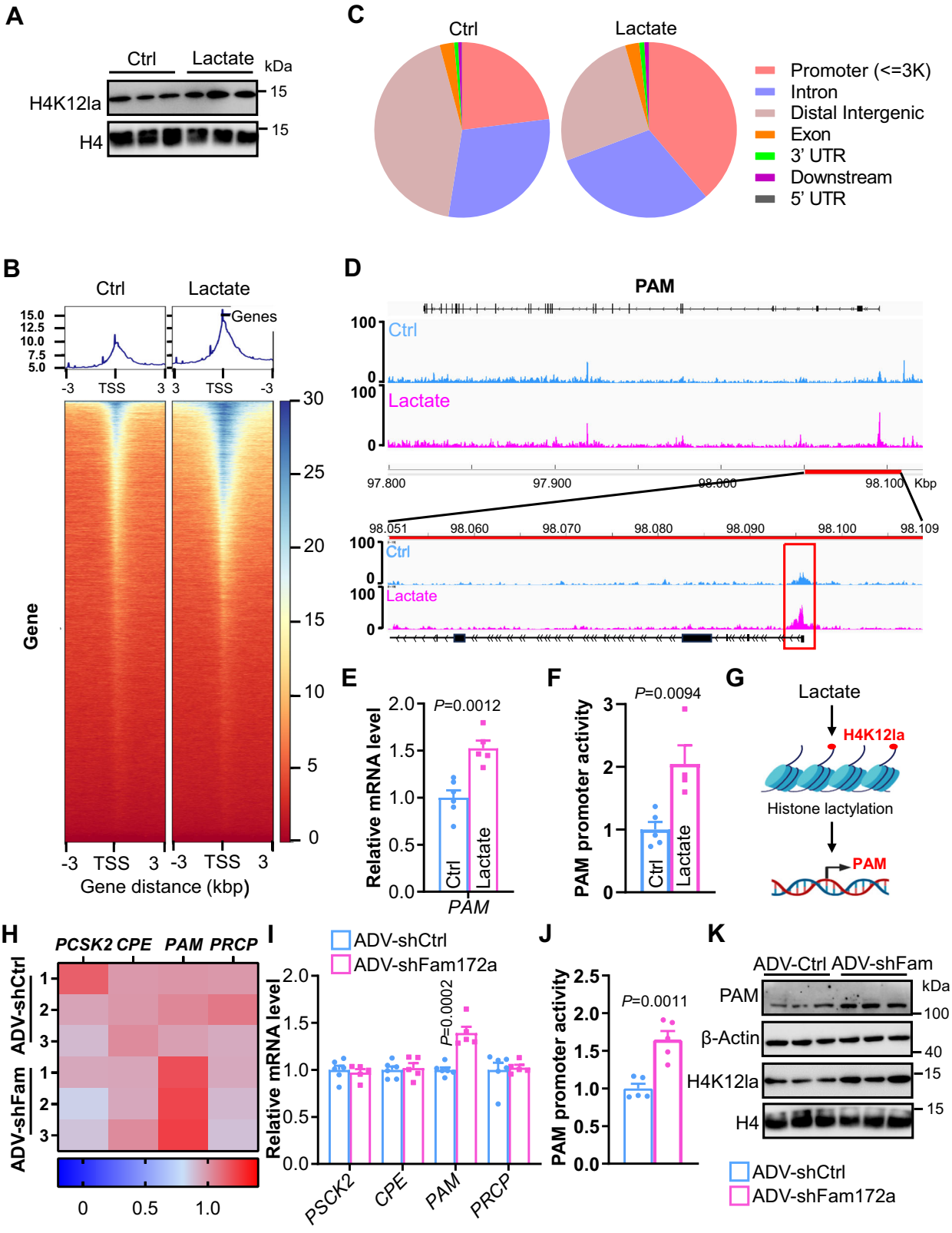

Western blot

Total protein was extracted from Neuro2a cells, separated by SDS-PAGE, and transferred to PVDF membranes. The membranes were then blocked with 5% non-fat milk, and incubated with rabbit anti-Fam172a (1:500), anti-LDHA (1:1000), anti-HK2 (1:1000) anti-PKM2 (1:1000), anti-PDK1 (1:1000), anti-PAM (1:1000), anti H4K12la (1:1000), anti H4 (1:1000) and anti *β-Actin* (1:1000) antibodies. After incubation with horseradish peroxidase-conjugated secondary antibody (1:10000), the membranes were exposed to the Supersignal West Femto Maximum Sensitivity Substrate (Thermo Fisher). Chemiluminescence was recorded with the GeneGnome system (Syngene, Cambridge, UK). Densitometric analysis of the western blot was performed via ImageJ.

Fig. 6 | Lactate regulates the transcriptional level of PAM through H4K12la. **A** Western blot analysis of H4K12la in neuro2a cells treated with NaCl or lactate at 37°C for 24 h. $n = 3$ cell cultures per group. **B** The binding density of H4K12la was visualized by deepTools: the heatmap presents the CUT&Tag tag counts on the different H4K12la binding peaks in neuro2a cells treated with NaCl or lactate at 37°C for 24 h, ordered by signal strength. **C** Genome-wide distribution of upregulated H4K12la-binding peaks in neuro2a cells treated with NaCl or lactate at 37°C for 24 h. **D** Genome browser tracks of CUT&Tag signals at the PAM target gene loci. **E** Neuro2a cells were treated with NaCl or latate at 37°C for 24 h, total RNA was then extracted, and the relative mRNA levels of the indicated genes were assessed. $n = 6$ (Ctrl) or 5 (Lactate) cell cultures per group. **F** Lactate treated neuro2a cells presented increased mouse PAM promoter activity. $n = 5$ (Ctrl) or 4 (Lactate) cell cultures per group. **G** A proposed working model for how lactate influenced the transcription of PAM. Created in BioRender. Chen, Z. (2024) https://BioRender.com/j97w406. **H** Neuro2a cells were transfected with ADV-shCtrl or ADV-shFam172a at 37°C for 48 h, after which RNA-Seq was performed. Heatmaps of POMC to α-MSH pathway target genes. n = 3 cell cultures per group. **I** Neuro2a cells were transfected with ADV-shCtrl or ADV-shFam172a at 37°C for 48 h, total RNA was then extracted, and the relative mRNA levels of the indicated genes were assessed. $n = 6$ (ADV-shCtrl) or 5 (ADV-shFam172a) cell cultures per group. **J** Knockdown of Fam172a in neuro2a cells increased mouse PAM promoter activity. $n = 5$ cell cultures per group. **K** Western blot analysis of PAM and H4k12la in neuro2a cells transfected with ADV-shCtrl or ADV-shFam172a at 37°C for 48 h. $n = 3$ cell cultures per group. Data are presented as mean ± SEM. two-tailed Student's *t*-test (**E, F, I, J**). Source data are provided as a Source Data file.

RNA sequencing

Total RNA was extracted from neuro2a cells infected with ADV-shCtrl or ADV-shFam172a via TRIzol reagent (Thermo Fisher). Quantity and quality of mRNA samples were examined via a Nanodrop system (ThermoFisher) and electrophoresis, respectively. RNA libraries were constructed using VAHTS® Universal V6 RNA-seq Library Prep Kit for Illumina Vazyme, according to the manufacturer's protocol, and paired-end reads were obtained on the NovaSeq 6000 platform. Quality of RNA-seq data was estimated using RSeQC (version 2.6.4). Differentially expressed genes were identified using the RankProd49 package in R based on P value < 0.01.

Seahorse XF assay

According to the manufacturer's instructions[46], ECAR was measured and recorded with a Seahorse XFe24 instrument. In brief, the ADV or plasmids treated cells were inoculated in XF24 cell culture plates and cultured for 24 h. Before the ECAR was measured, cell culture medium was replaced with XF base medium containing 2 mM glutamate, and cell culture plate was incubated in a CO_2-free incubator at 37°C for 1 h. Glycolytic function was determined by sequentially injecting glucose (10 mM), oligomycin A (1 μM) and 2-DG (50 mM) (The final concentrations in the wells are indicated).

Fam172a$^{loxP/loxP}$ and *PFKO* mice fed a HFD were anesthetized with isoflurane and decapitated, and their brains were quickly removed and placed in aCSF without glucose (120 mM NaCl, 3.5 mM KCl, 1.3 mM $CaCl_2$, 1 mM $MgCl_2$, 0.4 mM KH_2PO_4, 5 mM HEPES, 10 mM sucrose, and 4 g/L BSA) at 4°C. After the coronal planes of the superior and inferior margins of the hypothalamus were segregated, the brain tissue was fixed on a metal tray and sectioned into 250 μm thick coronal sections at 4°C. The Arc was removed using a 1 mm biopsy punches (Miltex, York, PA) and transferred to an XF Islet Capture Microplate containing glucose-free aCSF at 37°C. After incubation in a CO_2-free incubator at 37°C for 1 h, ECAR values were measured at baseline and after the addition of glucose (25 mM), oligomycin A (2.5 μM) or 2-DG (125 mM) (The final concentrations in the wells are indicated). ECAR was measured and recorded by a Seahorse XFe24 system[47].

Measurement of lactate levels

Arc of hypothalamus tissues and cultured neuro2a cells subjected to different treatments were homogenized with lysis buffer and sonicated at 300 W (3 s on and 7 s off) for 3 min on ice, followed by centrifugation at 12,000 g for 10 min at 4 °C. The supernatants were collected, and the lactate levels were measured using a Lactate Colorimetric Assay Kit (K607-100, BioVision) according to the manufacturer's instructions.

Histone extraction

Histones from cells were extracted using an acid-extraction protocol. In brief, tissues or cells were collected and resuspended in lysis buffer containing protease inhibitors for nucleus extraction. The nuclei were then resuspended in acid solutions (0.2 M HCl) at ice cold temperature for 30 min, followed by centrifugation at 12,000 × g for 15 min at 4 °C. The supernatants were collected, one-tenth of the volume of NaOH (2 M) was added, and the mixture was prepared for western blot analysis.

Dual luciferase reporter assay

LDHA, PDK1, PAM promoter-reporter plasmids and ADV-shFam172a or the corresponding controls were transfected into neuro2a cells. The cells were further cultured at 37 °C for 48 hours, and then were harvested to determine luciferase activity via reagents obtained from Promega. Another processing group, the PAM promoter-reporter plasmid or the control, was transfected into neuro2a cells. After 24 hours, the cell culture medium was replaced with fresh medium containing vehicle or lactate (25 mM). The cells were further cultured at 37 °C for 24 hours, and then were harvested to determine luciferase activity using reagents obtained from Promega. The activity of firefly luciferase was normalized to that of Renilla luciferase.

CUT&Tag

CUT&Tag was performed with a Hyperactive In-Situ ChIP Library Prep Kit for Illumina (pG-Tn5) (TD901, Vazyme Biotech) according to the manufacturer's instructions. In brief, NaCl or lactate (25 mM) treated neuro2a cells were collected and bounded to Concanavalin A–coated beads. Subsequently, cells were resuspended in antibody buffer and incubated with primary antibodies against H4K12la and secondary antibodies in order. The samples were incubated with pA-Tn5 transposase. After transposon activation and tagmentation, DNA was isolated, amplified, and purified to construct library. The library for sequencing was constructed and VAHTS DNA Clean Beads (N411, Vazyme Biotech) were used for purification steps. The library was quantified with VAHTS Library Quantification Kit for Illumina (Vazyme Biotech) and sequenced on an Illumina Novaseq 150PE system.

Measurement of α-MSH levels

Hypothalamic tissues were collected from Fam172a$^{L/L}$ and PFKO mice fed a HFD. Protein extracts were then prepared, and the concentrations were determined by using a BCA assay. α-MSH expression was measured with an EIA kit purchased from Phoenix Pharmaceuticals (Burlingame, CA). The hypothalamic peptide content was normalized to the total protein content[48].

RNAscope in situ hybridization (ISH)

For RNAscope mRNA detection, tissue preparations were as follows: PFA-fixed tissue was used to detect Fam172a mRNA, and the mice were perfused with PBS, followed by 4% PFA, and post-fixed in 4% PFA overnight. Brain tissues were cryoprotected using 20% and 30% sucrose solutions. 20 μm sections were cut on a microtome (Leica) and brain slides were stored at −80 °C before use. ISH was performed on tissue preparations according to the manufacturer's instruction for the

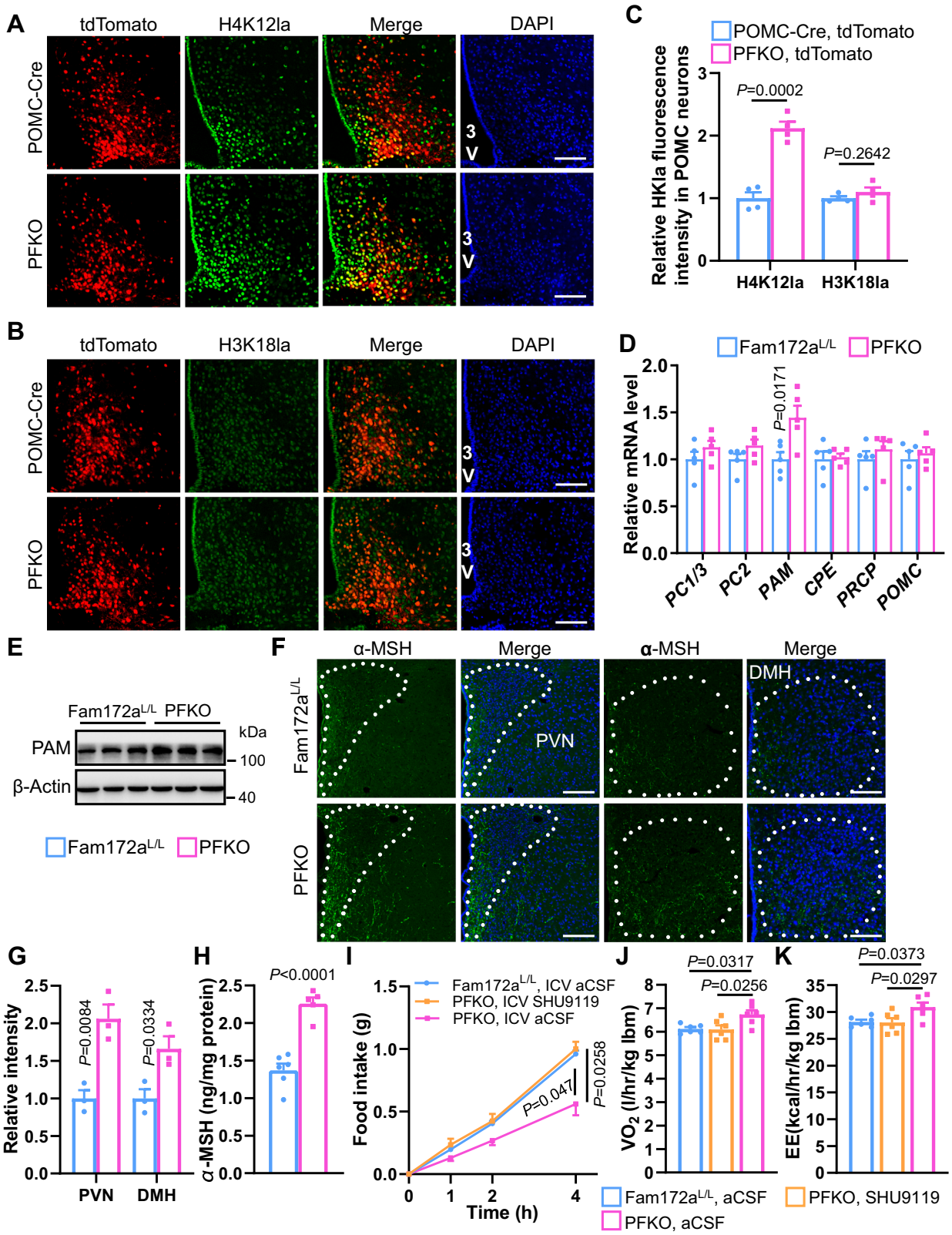

ACDBio RNAscope® 2.5 HD Reagent Kit-RED (Cat. no. 322350)[49] and the manufacturer's instructions for the PinpoRNATM RNA in-situ hybridization kit (Cat #: PIT1000, GD Pinpoease Biotech Co. Ltd.)[50] with slight modifications. The Fam172a probe (68652-B1) was purchased from Pinpoease Biotech. Images were acquired with an LSM980 confocal microscope (Carl Zeiss, Jena, Germany), and were processed using ImageJ (NIH, Bethesda, MD).

Statistical analysis

Statistical analyzes were performed in GraphPad Prism, version 9.0 (GraphPad Software, CA, USA). Data are presented as mean ± SEM. Two-tailed Student's *t* test was used for comparison between two groups. One- or two-way analysis of variance (ANOVA) followed by Bonferroni's or Tukey's *post hoc* test was used for comparisons of more than two groups, or multiple comparisons. $P < 0.05$ was considered

Fig. 7 | Disruption of Fam172a caused an increase of histone lactylation and α-MSH release in POMC neurons. A–C Immunofluorescence staining for H4K12la (green, **A**) or H3K18la (green, **B**) and tdTomato (red) was then performed on *POMC-Cre* or *PFKO* mouse brain sections. Quantification was then performed (**C**). Both *PFKO* and *POMC-Cre* mouse lines had been crossed with the *tdTomato reporter/Ail4* mice, so that the POMC neurons could be identified as tdTomato (red)-positive cells in the Arc nucleus. Cell nuclei were counterstained with DAPI (blue). $n = 4$ mice per group. 3 V, third ventricle. Scale bars, 100 μm. **D** Relative mRNA levels of α-MSH synthesis related genes in hypothalamus Arc of $Fam172A^{L/L}$ or *PFKO* mice. $n = 5$ cell cultures per group. **E** Western blot analysis of PAM in hypothalamus Arc of $Fam172A^{L/L}$ or *PFKO* mice. n = 3 mice per group. (**F**, **G**) Immunofluorescence staining for α-MSH (green) in brain sections from the PVN/DMH (**F**) and quantification of α-MSH fluorescence intensity (**G**). Cell nuclei were counterstained with DAPI (blue). $n = 3$ mice per group. Scale bars, 100 μm. (**H**) α-MSH levels in the hypothalamus of $Fam172A^{L/L}$ or *PFKO* mice. n = 6 ($Fam172a^{L/L}$) or 5 (*PFKO*) mice per group. **I** Effects of SHU9119 on PFKO induced inhibition of food intake, and cumulative food intake measured at 0 h, 1 h, 2 h and 4 h after central administration of SHU9119. $n = 10$ ($Fam172a^{L/L}$, ICV aCSF), 7 (PFKO, ICV SHU9119) or 7 (PFKO, ICV aCSF) mice per group. (**J**, **K**) Central administration of SHU9119 decreased oxygen consumption (VO2, **J**), and energy expenditure (EE, **K**) in PFKO mice. lbm, lean body mass. n = 6 mice per group. Data are presented as mean ± SEM. two-tailed Student's *t*-test (**C**, **D**, **G**, **H**), one-way ANOVA with Turkey's *post hoc test* (**J**, **K**), two-way ANOVA with Bonferroni's *post hoc* test (**I**). Source data are provided as a Source Data file.

statistically significant. The exact number of mice and cultures were indicated in the figure legend and representative data are shown.

Reporting summary

Further information on research design is available in the Nature Portfolio Reporting Summary linked to this article.

Data availability

The authors declare that all data supporting the findings of this study are available within this paper and its Supplementary Files. RNA-seq data is available with accession code GSE280694. Cut & Tag data is available with accession code GSE280695. Source data are provided with this paper. All data supporting the findings described in this manuscript is also available from the corresponding author upon request Source data are provided with this paper.

References

1. Rabinowitz, J. D. & Enerbäck, S. Lactate: the ugly duckling of energy metabolism. *Nat. Metab.* **2**, 566–571 (2020).
2. Zhang, W. et al. Lactate is a natural suppressor of RLR signaling by targeting MAVS. *Cell* **178**, 176–189.e115 (2019).
3. Daw, C. C. et al. Lactate elicits ER-mitochondrial Mg2+ dynamics to integrate cellular metabolism. *Cell* **183**, 474–489.e417 (2020).
4. Brooks, G. A. The science and translation of lactate shuttle theory. *Cell Metab.* **27**, 757–785 (2018).
5. McCarthy, S. F., Islam, H. & Hazell, T. J. The emerging role of lactate as a mediator of exercise-induced appetite suppression. *Am. J. Physiol.-Endocrinol. Metab.* **319**, E814–E819 (2020).
6. Lu, L. et al. MCT2 Expression and lactate influx in anorexigenic and orexigenic neurons of the arcuate nucleus. *PLoS ONE* **8**, e62532 (2013).
7. Elizondo-Vega, R. et al. Inhibition of hypothalamic MCT4 and MCT1–MCT4 expressions affects food intake and alters orexigenic and anorexigenic neuropeptide expressions. *Mol. Neurobiol.* **57**, 896–909 (2019).
8. Ou, Z. et al. A GPR17-cAMP-lactate signaling axis in oligodendrocytes regulates whole-body metabolism. *Cell Rep.* **26**, 2984–2997.e2984 (2019).
9. Hagihara, H. et al. Protein lactylation induced by neural excitation. *Cell Reports* **37**, 109820 (2021).
10. Pan, R.-Y. et al. Positive feedback regulation of microglial glucose metabolism by histone H4 lysine 12 lactylation in Alzheimer's disease. *Cell Metab.* **34**, 634–648.e636 (2022).
11. Rho, H., Terry, A. R., Chronis, C. & Hay, N. Hexokinase 2-mediated gene expression via histone lactylation is required for hepatic stellate cell activation and liver fibrosis. *Cell Metab.* **35**, 1406–1423.e1408 (2023).
12. Lin, X. et al. Augmentation of scleral glycolysis promotes myopia through histone lactylation. *Cell Metab.* **36**, 511–525 (2024).
13. Li LX, et al. Molecular cloning of a novel gene, C5orf21 gene and its roles in diabetic macroangiopathy. *Zhonghua Yi Xue Za Zhi* (2009).
14. Li, L. X. et al. Identification of the novel protein FAM172A, and its up-regulation by high glucose in human aortic smooth muscle cells. *Int. J. Mol. Med.* **26**, 483–490 (2010).
15. Bélanger, C. et al. Dysregulation of cotranscriptional alternative splicing underlies CHARGE syndrome. *Pro. Nati. Acad. Sci. USA.* **115**, E620–E629 (2018).
16. Liu, T., Xu, Y., Yi, C.-X., Tong, Q. & Cai, D. The hypothalamus for whole-body physiology: from metabolism to aging. *Protein Cell* **13**, 394–421 (2021).
17. Cone, R. D. Anatomy and regulation of the central melanocortin system. *Nat. Neurosci.* **8**, 571–578 (2005).
18. Kumar, D., Mains, R. E. & Eipper, B. A. 60 YEARS OF POMC: From POMC and α-MSH to PAM, molecular oxygen, copper, and vitamin C. *J. Mol. Endocrinol.* **56**, T63–T76 (2016).
19. Bousquet-Moore, D., Mains, R. E. & Eipper, B. A. Peptidylglycine α-amidating monooxygenase and copper: a gene–nutrient interaction critical to nervous system function. *J. Neurosci. Res.* **88**, 2535–2545 (2010).
20. Czyzyk, T. A. et al. Deletion of peptide amidation enzymatic activity leads to edema and embryonic lethality in the mouse. *Developmental Biol.* **287**, 301–313 (2005).
21. Huyghe, J. R. et al. Exome array analysis identifies new loci and low-frequency variants influencing insulin processing and secretion. *Nat. Genet.* **45**, 197–201 (2012).
22. Steinthorsdottir, V. et al. Identification of low-frequency and rare sequence variants associated with elevated or reduced risk of type 2 diabetes. *Nat. Genet.* **46**, 294–298 (2014).
23. Bélanger, C., Cardinal, T., Leduc, E., Viger, R. S. & Pilon, N. CHARGE syndrome-associated proteins FAM172A and CHD7 influence male sex determination and differentiation through transcriptional and alternative splicing mechanisms. *FASEB J.* **36**, e22176 (2022).
24. Sallis, S. et al. The CHARGE syndrome-associated protein FAM172A controls AGO2 nuclear import. *Life Sci. Alliance* **6**, e202302133 (2023).
25. Salgado, M. et al. GKRP-dependent modulation of feeding behavior by tanycyte-released monocarboxylates. *Theranostics* **12**, 1518–1536 (2022).
26. Wu, Y. et al. Hippocampal lactate-infusion enhances spatial memory correlated with monocarboxylate transporter 2 and lactylation. *Brain Sciences* **14**, 327 (2024).
27. Joseph, C. G. Design, synthesis, and characterization of peptides and peptidomimetics for mouse melanocortin receptors (2016).
28. Lam, C. K. L., Chari, M., Wang, P. Y. T. & Lam, T. K. T. Central lactate metabolism regulates food intake. *Am. J. Physiol.-Endocrinol. Metab.* **295**, E491–E496 (2008).
29. Chen, M. Y. et al. Deletion of accelerates advanced atherosclerosis and induces plaque instability. *Atherosclerosis* **333**, 39–47 (2021).
30. Semenza, G. L. Hypoxia-inducible factors in physiology and medicine. *Cell* **148**, 399–408 (2012).

31. Sharma, D., Singh, M. & Rani, R. Role of LDH in tumor glycolysis: regulation of LDHA by small molecules for cancer therapeutics. *Semin. Cancer Biol.* **87**, 184–195 (2022).
32. Warburg, O. Origin of Cancer Cells. *Science* **123**, 309–314 (1956).
33. Bonvento, G. & Bolaños, J. P. Astrocyte-neuron metabolic cooperation shapes brain activity. *Cell Metab.* **33**, 1546–1564 (2021).
34. Zhang, Y. et al. An RNA-sequencing transcriptome and splicing database of glia, neurons, and vascular cells of the cerebral cortex. *J. Neurosci.* **34**, 11929–11947 (2014).
35. Burdakov, D., Luckman, S. M. & Verkhratsky, A. Glucose-sensing neurons of the hypothalamus. *Philos. Trans. R. Soc. B: Biol. Sci.* **360**, 2227–2235 (2005).
36. Lhomme, T. et al. Tanycytic networks mediate energy balance by feeding lactate to glucose-insensitive POMC neurons. *J. Clin. Invest.* **131**, e153279 (2021).
37. Beard, E., Lengacher, S., Dias, S., Magistretti, P. J. & Finsterwald, C. Astrocytes as key regulators of brain energy metabolism: new therapeutic perspectives. *Front. Physiol.* **12**, 825816 (2022).
38. Órdenes, P. et al. Lactate activates hypothalamic POMC neurons by intercellular signaling. *Sci. Rep.* **11**, 21644 (2021).
39. Yoon, N. A. et al. UCP2-dependent redox sensing in POMC neurons regulates feeding. *Cell Rep.* **41**, 111894 (2022).
40. Zhang, D. et al. Metabolic regulation of gene expression by histone lactylation. *Nature* **574**, 575–580 (2019).
41. Sun, S. et al. Lactic acid-producing probiotic saccharomyces cerevisiae attenuates ulcerative colitis via suppressing macrophage pyroptosis and modulating gut microbiota. *Front. Immunol.***12**, 777665 (2021).
42. Balthasar, N. et al. Leptin Receptor Signaling in POMC Neurons Is Required for Normal Body Weight Homeostasis. *Neuron* **42**, 983–991 (2004).
43. Madisen, L. et al. A robust and high-throughput Cre reporting and characterization system for the whole mouse brain. *Nat. Neurosci.* **13**, 133–140 (2009).
44. Chen, Z. et al. Deficiency of ER Ca2+ sensor STIM1 in AgRP neurons confers protection against dietary obesity. *Cell Rep.* **37**, 109868 (2021).
45. Zhang, Y. et al. Neuregulin4 acts on hypothalamic ErBb4 to excite oxytocin neurons and preserve metabolic homeostasis. *Adv. Sci.* **10**, 2204824 (2023).
46. Rahman, M. H. et al. Astrocytic pyruvate dehydrogenase kinase-2 is involved in hypothalamic inflammation in mouse models of diabetes. *Nat. Commun.* **11**, 5906 (2020).
47. Qi, G. et al. ApoE4 Impairs Neuron-Astrocyte Coupling of Fatty Acid Metabolism. *Cell Rep.* **34**, 108572 (2021).
48. Zhang, Y. et al. Hypothalamic extended synaptotagmin-3 contributes to the development of dietary obesity and related metabolic disorders. *Proc. Natl Acad. Sci.* **117**, 20149–20158 (2020).
49. Cong, Q., Soteros, B. M., Wollet, M., Kim, J. H. & Sia, G.-M. The endogenous neuronal complement inhibitor SRPX2 protects against complement-mediated synapse elimination during development. *Nat. Neurosci.* **23**, 1067–1078 (2020).
50. Liang, Y. et al. Gene activation guided by nascent RNA-bound transcription factors. *Nat. Commun.* **13**, 7329 (2022).

Acknowledgements

This research was supported by grants from the National Science Foundation of China (82200944, 82325010, 82270894, 82470818, 82100908), the China Postdoctoral Science Foundation Funded Project (2022M712107), Major Natural Science Project of the Scientific Research and Innovation Plan of Shanghai Municipal Commission of Education (2023ZKZD17), the Shanghai Post-doctoral Excellence Program (2022409) and the Shanghai Sixth People's Hospital Foundation (ynqn202206, ynms202404).

Author contributions

Z.C. designed and performed the experiments, analyzed the data, and wrote the paper. Y.Z. and C.H. conceived the study, designed the experiments, and revised the paper. B.W. helped perform the experiments, and H.Z. helped analyze the data. L. Z., R.Z., and L.L. provided helpful suggestions about the experiments. Y.Z. and C.H. directed the research. All the authors commented on the paper.

Competing interests

The authors declare no competing interests.

Additional information

Supplementary information The online version contains supplementary material available at https://doi.org/10.1038/s41467-024-54488-4.

Correspondence and requests for materials should be addressed to Yi Zhang or Cheng Hu.

Peer review information *Nature Communications* thanks Maria Garcia-Robles and the other anonymous reviewer(s) for their contribution to the peer review of this work. A peer review file is available.